

<https://doi.org/10.1038/s42004-024-01185-4>

A facile DNA coacervate platform for engineering wetting, engulfment, fusion and transient behavior

Check for updates

Wei Liu¹, Jie Deng², Siyu Song¹, Soumya Sethi¹ & Andreas Walther¹✉

Biomolecular coacervates are emerging models to understand biological systems and important building blocks for designer applications. DNA can be used to build up programmable coacervates, but often the processes and building blocks to make those are only available to specialists. Here, we report a simple approach for the formation of dynamic, multivalency-driven coacervates using long single-stranded DNA homopolymer in combination with a series of palindromic binders to serve as a synthetic coacervate droplet. We reveal details on how the length and sequence of the multivalent binders influence coacervate formation, how to introduce switching and autonomous behavior in reaction circuits, as well as how to engineer wetting, engulfment and fusion in multi-coacervate system. Our simple-to-use model DNA coacervates enhance the understanding of coacervate dynamics, fusion, phase transition mechanisms, and wetting behavior between coacervates, forming a solid foundation for the development of innovative synthetic and programmable coacervates for fundamental studies and applications.

Membraneless organelles (MLOs), also known as biomolecular condensates, form through liquid–liquid phase separation (LLPS) within cells and have been shown to play a crucial role in regulating biological functions^{1–3}. Unlike traditional membrane-bound organelles, MLOs such as nucleoli, stress granules, and P-bodies function in the absence of a surrounding lipid bilayer. They are often formed by proteins or complexes of proteins and nucleic acids^{4–6}. The unique properties of MLOs are predominantly driven by an array of weak interactions, including protein–protein, protein–RNA, electrostatic, and hydrophobic interactions, culminating in dynamic liquid properties^{7–9}. These liquid characteristics influence the spatial organization, phase transition, and molecular interactions within cells, thereby regulating diverse cellular activities, including gene expression, cell adhesion, and cargo recruitment^{10–12}.

Inspired by natural LLPS-driven organelles, the fabrication of bio-inspired LLPS systems, consisting of DNA, RNA, and proteins, has gained much ground in order to better understand biological systems using defined model systems, as well as for generating functional materials relevant to the molecular systems engineering world^{13–17}. Despite the progress, many open questions remain, for instance, regarding the interactions between coacervates of different natures and of coacervates with soft interfaces. Interesting progress has also been made with respect to the uptake of coacervates

into liposomes or cells or, very recently, regarding LLPS in fibrillar environments^{18–20}.

DNA is an appealing building block to build up coacervates due to the programmable nature of interactions²¹. Various strategies have been employed to construct DNA coacervates and droplets, including the use of hybridization-mediated assembly of DNA nanostars or temperature-induced phase segregation and trapping of DNA^{16,22–25}. These all-DNA artificial cell models can exhibit liquid-like behavior, beneficial to study adhesion, fission, fusion, and wetting^{26–32}. For instance, Takinoue and co-workers investigated the impact of DNA sequences on the fusion dynamics of liquid-like droplets at elevated temperatures (above 43 °C)²⁸. However, many of the approaches require specialist knowledge of DNA assembly techniques and well-designed annealing protocols, whereas simple mix-and-use protocols at one temperature would be very desirable.

In this study, we report an easy-to-use platform for all-DNA coacervates utilizing single-stranded DNA (ssDNA) components and multivalency-driven LLPS at physiological temperature (Fig. 1). We show that a series of palindromic domains can be flexibly hybridized to long ssDNA homopolymers composed solely of adenine nucleotides (polyA) to trigger coacervate formation, and to study dynamics as a function of the type of palindromic binder. Through the integration of DNA or RNA strands, we establish switchable systems for the controlled assembly and disassembly of

¹Life-Like Materials and Systems, Department of Chemistry, University of Mainz, Duesbergweg 10-14, 55128 Mainz, Germany. ²School of Chemistry and Chemical Engineering, Huazhong University of Science and Technology, Luoyu Road 1037, 430074 Wuhan, China. ✉e-mail: andreas.walther@uni-mainz.de

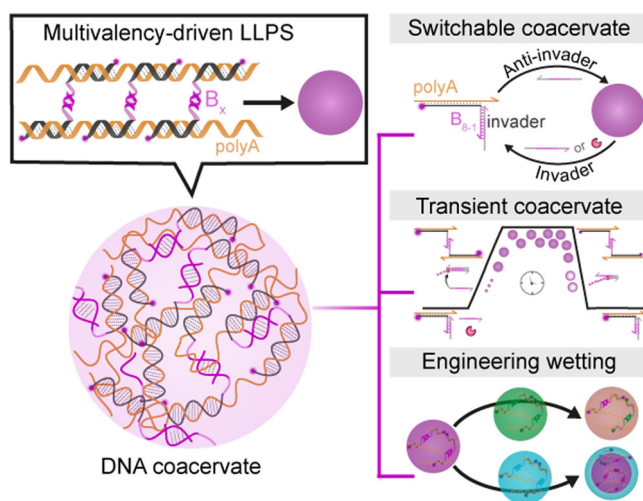


Fig. 1 | Multivalency-driven all-DNA coacervates: coacervate preparation, switching, autonomous behavior, and engineered wetting for multiphase structures. DNA coacervates are prepared via multivalency-driven liquid-liquid phase separation (LLPS) between a ssDNA polymer (polyA) and shorter self-complementary binders (B_x). The introduction of DNA or RNA invaders triggers the formation of switchable and transient coacervates. Using two distinct coacervates with different palindromic domains allows controlling multiphase structures through engineering wetting.

coacervates. This advancement enables the realization of a transient, autonomous coacervate system³³. Furthermore, the selective exploitation of the distinctive dynamic properties conferred by various palindromic domains allows to engineer multiphase structures through tailored wetting mechanisms. We anticipate that the facile formation mechanism and the flexible design of different dynamic behaviors of these DNA coacervates will pave the way for the engineering of functional DNA-based coacervates, with great potential to be followed up by non-experts.

Results

Formation of multivalency-driven coacervates

Our strategy for the fabrication of all-DNA coacervates employs a straightforward multivalency-driven LLPS approach based on the combination of a ssDNA homopolymer (polyA; A = adenine) and shorter binders (B_x) containing palindromic domains and a T_{30} (T = thymine) domain for hybridization to the polyA backbone (Fig. 2a). The DNA homopolymer A_{1500} was synthesized using terminal deoxynucleotidyl transferase (TdT)-catalyzed polymerization to feature 1500 repeating units^{34,35}. Similar polyAs are, however, also available commercially. The binders, B_x , typically feature four components: (1) the complementary segment T_{30} ensuring hybridization to the polymer A_{1500} (melting temperature, $T_m(A_{30}/T_{30}) = 62.8$ °C at 10 mM Mg^{2+} , 50 mM Na^+ , by IDT), (2) an intermediate spacer providing both flexibility and a toehold (S_7), (3) the palindromic domain, P_x , facilitating multivalent interactions, and (4) a dye label. These structures are hence composed of T_{30} - S_7 - P_x (or shorter B_x), whereby x signifies the length of the palindrome and thus the strength of the interaction. The strength of the palindrome also depends on the GC content. The table listing the T_m in Fig. 2b gives a rough correlation of the binder strength.

We designed eight distinct binder strands (T_{30} - S_7 - $P_x = B_x$), each characterized by a unique sequence and varying length of the palindromic domain (Fig. 2b). Through this approach, we aimed to understand the influence of these two factors (GC content and palindromic length) on the formation and dynamics of spherical coacervates. Coacervate systems were typically assembled by mixing B_x with A_{1500} in a molar ratio of 25:1 at 1.5 μM T_{30} - S_7 - P_x and 0.06 μM A_{1500} at 37 °C in a buffer containing 10 mM Mg^{2+} and 50 mM K^+ (pH = 7.9). Note that 0.06 μM A_{1500} is equivalent to 3 μM A_{30} , and hence the B_x segments can occupy 50% of all A repeat units in A_{1500} . Confocal laser scanning microscopy (CLSM) shows nicely spherical

coacervates for five of the eight systems (Fig. 2c, d; Supplementary Data 1). The system featuring the shortest P_x , comprised of merely four nucleotides (nt) and a low GC content (P_{4-1}), presents no distinguishable structure formation. Systems with the longest P_x , containing 10 or 12 nt (P_{10} , P_{12}), display excessive aggregation into non-spherical structures. This behavior roughly correlates with the T_m of the individual palindromes, but the multivalent strengthening needs to be considered as well.

The absence of coacervate formation in the A_{1500}/P_{4-1} system ($T_{m,P_{4-1}} = 0$ °C) arises from the feeble multivalent binding due to the low GC content. Even though the other shorter P_x systems ($x = 4-2, 6, 8-1, 8-2, 8-3$) have also calculated $T_m < 28$ °C, hence still significantly lower than the system temperature of 37 °C, they still lead to the formation of well-defined spherical coacervates due to efficient multivalency effects. This indicates a dynamic nature and binding/unbinding dynamics. In contrast, the aggregation in systems incorporating the longest P_x strands ($x = 10, 12$) with $T_m = 38.7$ and 41.9 °C can be attributed to the excessively rigid multivalent interactions without significant internal dynamics for rearrangement into spherical structures. Hence, for the fabrication of spherical all-DNA coacervate via multivalency-driven LLPS, the optimum length of P_x containing four GC bases lies in the approximate range of 4–8 nt in total (Fig. 2c). This balances phase separation and sufficient rebinding dynamics on a multivalency level, yielding the desired spherical structural output.

We monitored a mixture of A_{1500} and B_{8-1} at 37 °C for visual tracking of the coacervate formation. After 0.5 h, a population of small coacervates with an average diameter of 0.7 μm appears. These small coacervates rapidly coalesce, gradually increase in size, and transform into larger entities with an average diameter of ca. 2.8 μm within 1 h. In the following 30 h, these structures continue to progressively coalesce and evolve into well-defined coacervates with ca. 8.8 μm diameter (Fig. 2e, Supplementary Fig. 1). This coalescence and growth further highlight the dynamic behavior within the phase-separated coacervate state. Fluorescence recovery after photobleaching (FRAP) measurements reveal a partial, limited recovery within 1.5 h post bleaching for the three coacervates with 8 nt in the palindrome. At the same time, partial fusion events can be clearly observed (Supplementary Fig. 2; arrows therein highlight fusion events; Supplementary Fig. 3 shows the minor effect of palindromic domains with different lengths = 4, 6, 8 nt). Hence, these coacervates are sufficiently dynamic to allow for fusion. Most interestingly, the coacervates formed by B_{8-2} show the quickest recovery at the coacervate surface. Hence, despite the strong similarities in the different binders of the B_{8-y} series, subtle differences in behavior can occur.

DNA- and RNA-triggered coacervate dynamics: switchable and transient systems

In the above investigation, we discussed the mechanism and conditions guiding the formation of our multivalency-driven coacervates. To achieve switchable and transient coacervate systems, we employed tools from DNA and RNA nanoscience to coacervates formed with the binder B_{8-1} . For the establishment of switchable coacervates, we introduced a DNA invader consisting of a domain complementary to the S_7 - P_{8-1} segment of the binder, along with an additional dangling overhang acting as a toehold for subsequent reactions (Fig. 3a; all sequences in Table S1). The addition of this invader to already formed coacervates disengages the multivalent interactions via strand displacement of the P_x/P_x palindrome. CLSM images demonstrate the disappearance of the coacervates upon the addition of the DNA invader in less than 10 minutes (Fig. 3b). Furthermore, the introduction of an additional DNA anti-invader, which can hybridize with the DNA invader at its dangling overhang, triggers displacement of the invader and the re-engagement of the palindromic hybridization site followed by reassembly of the coacervate. This process enables simple isothermal switching of the DNA coacervates.

This concept can be extended to an RNA invader capable of complementary interaction with the S_7 - P_{8-1} segment of the binder (Fig. 3c, d, Supplementary Fig. 4). When RNA invaders are introduced, the coacervates disassemble rapidly in less than 10 minutes. Coacervate reassembly occurs upon the addition of RNase H, which specifically degrades RNA hybridized

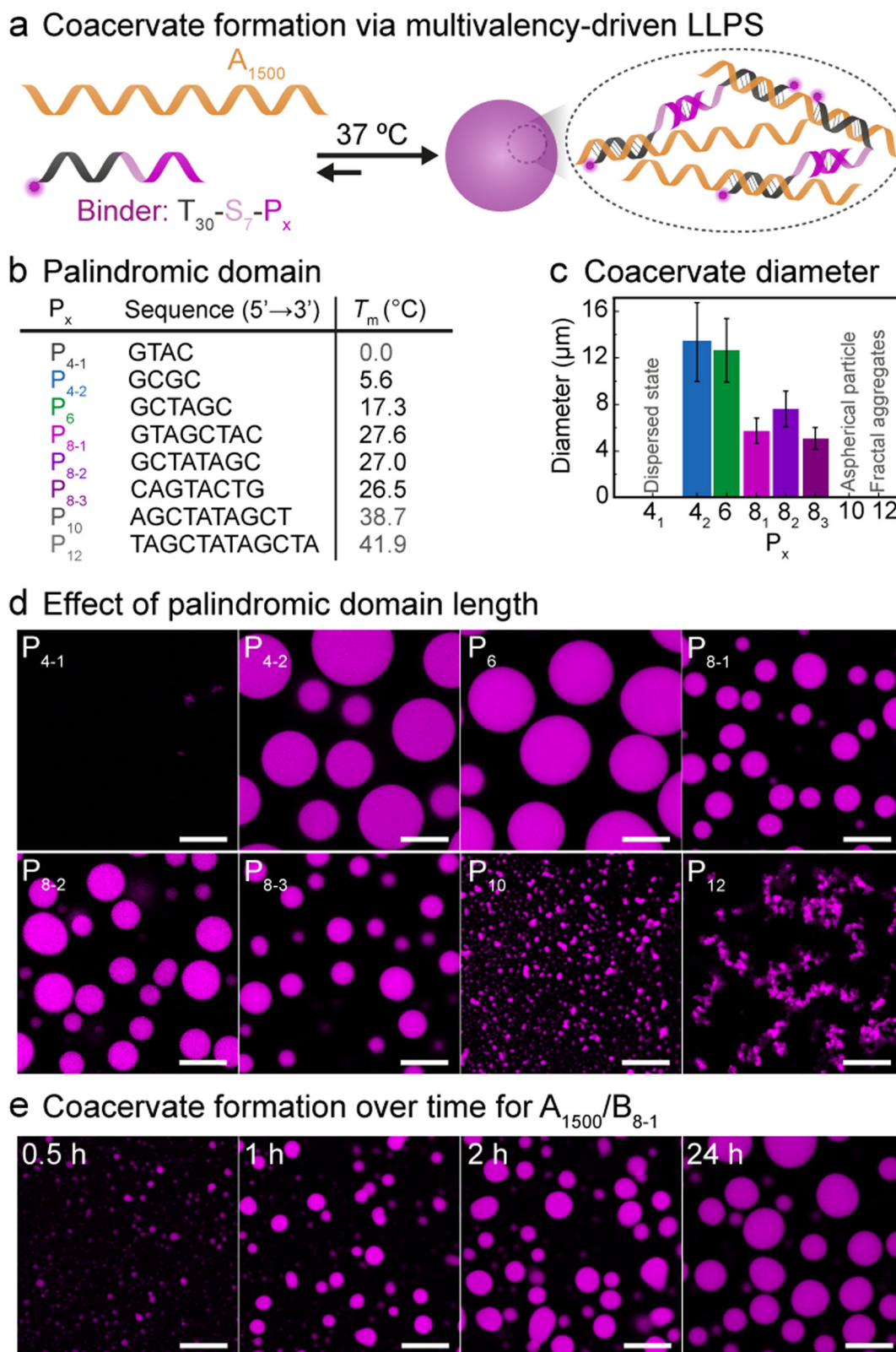
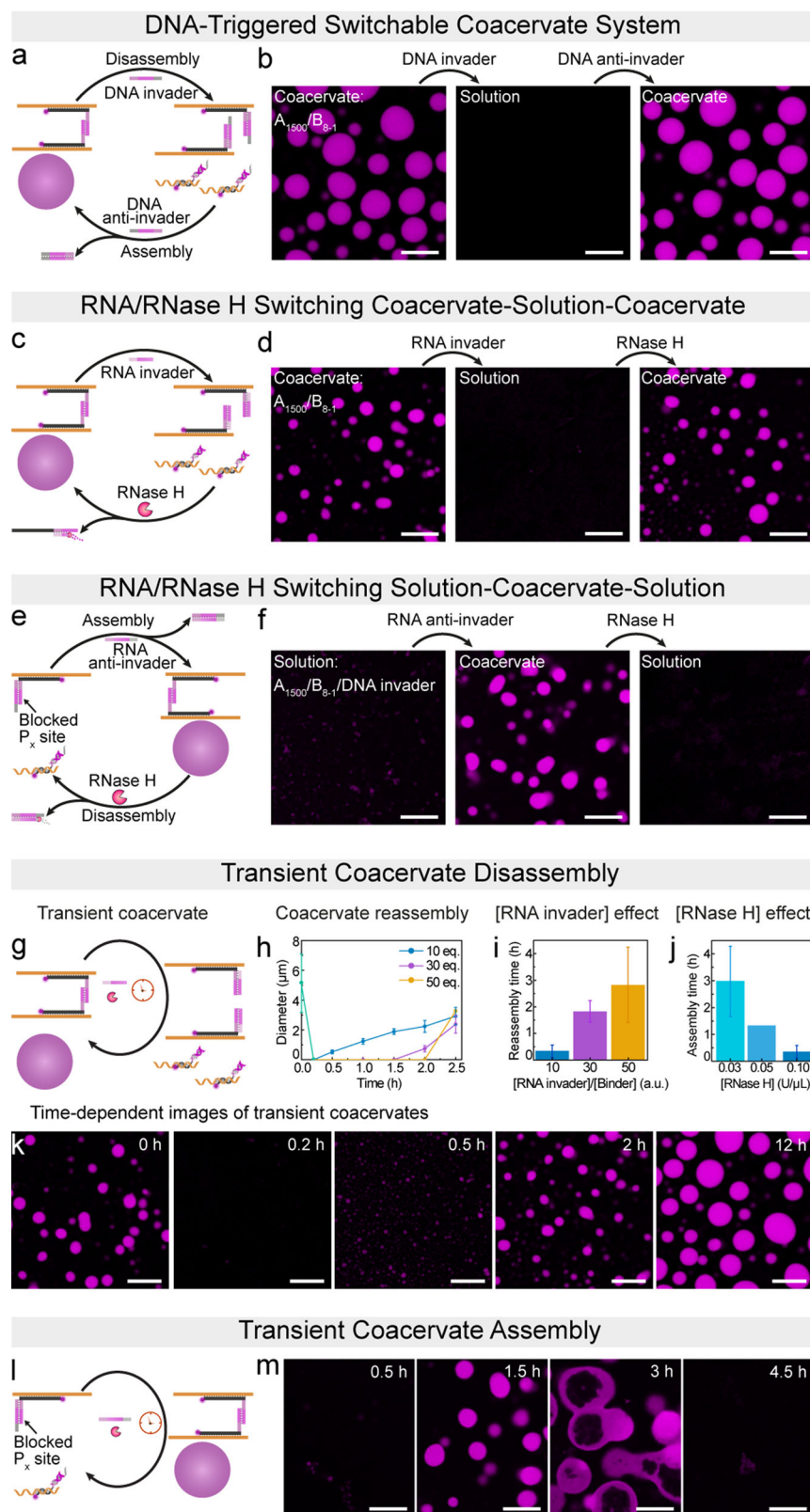


Fig. 2 | Mechanism of the formation of multivalency-driven coacervates and the palindromic domain effect on the formation. **a** Multivalency-driven coacervates by a long ssDNA (A_{1500}) mixed with short binder ssDNA consisting of a complementary strand T_{30} , a spacer S_7 and a palindromic multivalency domain P_x . **b** Sequences and melting temperatures (T_m) of the palindromic domains at 10 mM Mg^{2+} . **c** Size distribution of coacervates in systems containing 0.06 μM A_{1500} and

1.5 μM binder at 37 °C after a 4 h reaction period with various palindromic domains. Error bars correspond to standard deviations of ca. 150 coacervates. **d** CLSM images of systems containing 0.06 μM A_{1500} and 1.5 μM binder at 37 °C after a 4 h reaction period with different palindromic domains. **e** Time-dependent CLSM images of A_{1500}/B_{8-1} . The fluorescent labels are on the B_x . The experiments were conducted at 37 °C with gentle rotation at 80 rpm. Scale bars: 10 μm .

Fig. 3 | DNA- and RNA-triggered switchable coacervates and RNA-regulated transient coacervates. **a** and **b** Illustration and CLSM images of DNA-triggered switchable coacervate systems. 2.25 μM (1.5 eq.) of DNA invader was introduced to the coacervates formed from 0.06 μM A_{1500} and 1.5 μM (1.0 eq.) of B_{8-1} , resulting in the disassembly of the coacervates. Subsequently, the addition of 3 μM (2.0 eq.) of DNA anti-invader caused the reformation of coacervates. **c** and **d** Illustration and CLSM images of RNA-triggered switching between coacervate and solution states. 4.5 μM (3 eq.) of RNA invader was introduced to the coacervates formed from 0.06 μM A_{1500} and 1.5 μM (1.0 eq.) of B_{8-1} , resulting in the disassembly of the coacervates. Subsequently, the addition of 0.1 $\text{U } \mu\text{L}^{-1}$ of RNase H triggered the assembly of coacervates. **e** and **f** Illustration and CLSM images of RNA-triggered switchable coacervate of solution-to-coacervate-to-solution. 15 μM (10 eq.) of RNA anti-invader was introduced into the complex comprising 0.06 μM A_{1500} , 1.5 μM B_{8-1} , and 2.25 μM DNA invader, leading to the assembly of the coacervates. Subsequently, the addition of 0.1 $\text{U } \mu\text{L}^{-1}$ of RNase H caused the coacervates to disassemble into a homogeneous solution. A few tiny objects in the initial state may be due to the incomplete dissolution of the dye-bearing strand adsorbed in the microscopy chamber. **g–k** RNA-regulated transient coacervate disassembly with the introduction of RNA invader and RNase H: **g** Schematic illustration. **h** Time-dependent plot of the transient coacervates with tunable reassembly times by varying the concentration of RNA invaders. The green line indicates starting from a similar population of coacervates. Error bars are the standard deviation of ca. 20 droplet counts. **i** Controlled reassembly times via the concentration ratios of RNA invader/binder. Error bars correspond to standard deviations from duplicates. **j** Controlled reassembly times via the RNase H concentrations. Error bars correspond to standard deviations from duplicates. **k** Time-dependent CLSM images of transient coacervates with 15 μM (10 eq.) RNA invader and 0.1 $\text{U } \mu\text{L}^{-1}$ RNase H. **l** and **m** RNA-regulated transient coacervate assembly with the introduction of RNA anti-invader and RNase H: **l** Schematic illustration. **m** Time-dependent CLSM images of transient coacervates with 45 μM (30 eq.) RNA anti-invader and 0.1 $\text{U } \mu\text{L}^{-1}$ RNase H. The experiments were conducted at 37 $^{\circ}\text{C}$ with gentle rotation at 80 rpm. Scale bars: 10 μm .



with DNA. A toehold is no longer needed as for the DNA invader. The use of an enzyme allows, in principle, to fine-tune the kinetics of the re-engagement by simply changing its concentration. Furthermore, the switching process can be inverted by introducing an RNA anti-invader that removes a blocker strand from the B_x domain to trigger assembly. Subsequent addition of RNase H thereafter affords disassembly of the

coacervate systems by degradation of the RNA anti-invader and subsequent reblocking of the B_x with the newly liberated original ssDNA block strand (Fig. 3e,f).

Building upon the RNA-triggered switchable coacervate systems, we asked whether autonomous and transient coacervate dissolution, as well as coacervate formation, would be possible by the addition of RNA trigger

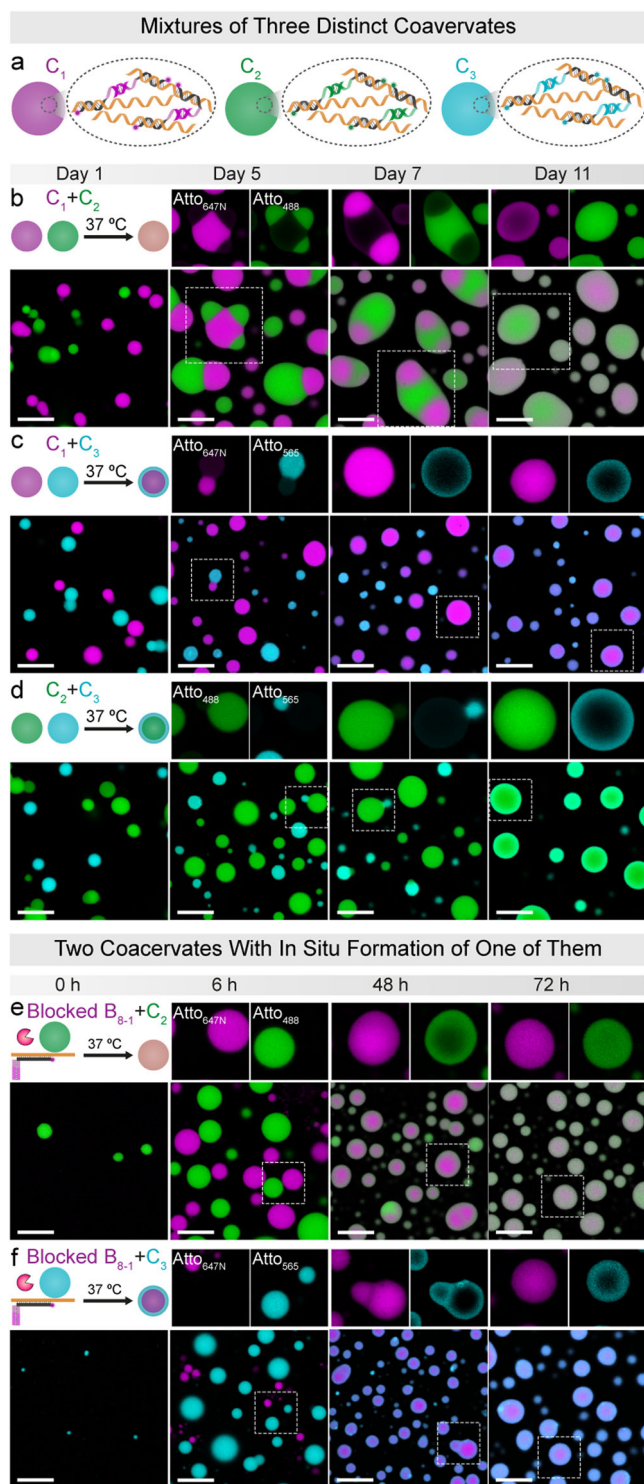


Fig. 4 | Engineering wetting between coacervates formed with diverse palindromic sequences at 37 °C. The coacervates were prepared using a mixture containing a final concentration of 0.06 μM of A_{1500} and 1.5 μM of the respective B_x . **a** Illustration of three distinct coacervate structures (C_1 in magenta, C_2 in green, and C_3 in cyan) synthesized from different binders (Atto_{647N}- B_{8-1} , Atto₄₈₈- B_{8-2} , and Atto₅₆₅- B_{8-3}) with various palindromic sequences (P_{8-1} , P_{8-2} , and P_{8-3} , as shown in Fig. 2b, c). The experiments were performed at 37 °C with gentle rotation at 80 rpm unless otherwise specified. **b** Wetting behavior between distinct C_1 and C_2 , leading to the formation of mixed coacervates. **c** Wetting behavior between C_1 and C_3 , resulting in the formation of core-shell structures. **d** Wetting behavior between C_2 and C_3 , contributing to the formation of core-shell structures. The experiments were carried out at 37 °C without rotation to minimize collisions. **e** Behavior during RNase H-initiated, slow coacervation of C_1 in a dispersion of preformed C_2 . 0.1 $\text{U } \mu\text{L}^{-1}$ RNase H and preformed C_2 were introduced into the complex comprising 0.06 μM A_{1500} , 1.5 μM of B_{8-1} , and 2.25 μM RNA invader. **f** Behavior during RNase H-initiated, slow coacervation of C_1 to preformed C_3 . 0.1 $\text{U } \mu\text{L}^{-1}$ RNase H and preformed C_3 were introduced into the complex comprising 0.06 μM A_{1500} , 1.5 μM of B_{8-1} , and 2.25 μM RNA invader. The experiments were conducted at 37 °C with gentle rotation at 80 rpm. Scale bars: 10 μm .

are observed because of the gradual degradation of the RNA invader by the already present RNase H. As RNA degradation continues, the reformation of well-defined coacervates occurs (Fig. 3h, k; Supplementary Data 1). Importantly, the reassembly time (defined as the point where coacervates reappear in CLSM) of these transient coacervates can be adjusted within a range of 0.3–2.9 h by either augmenting the quantity of RNA invader or reducing the concentration of RNase H (Fig. 3i, j; Supplementary Figs. 5 and 6; Supplementary Data 1).

The opposite pathway, i.e., transient coacervates, can be accomplished by integrating the $A_{1500}/B_{8-1}/\text{DNA}$ -invader complex with an excess of RNA anti-invader and a low concentration of RNase H (Fig. 3l). The RNA anti-invader quickly removes the DNA strand blocking the multivalent interaction, and thereby activated coacervation. By balancing the competition between anti-invader/invader hybridization and anti-invader degradation by RNase H and allowing the necessary time for coacervate formation, well-defined coacervate structures are observed after 1.5 h (Fig. 3m, Supplementary Fig. 7). After 3 h, these coacervates gradually disappear. Strikingly, hollow capsules appear, which indicates entrapment of the RNase H due to affinity to RNA (and potentially DNA) inside the coacervates and degradation from the inside. The relatively high stability of the vacuoles without diffusion to the surface likely originates from the viscoelastic character of the coacervates with limited dynamics (FRAP in Supplementary Fig. 2). Such vacuole formation has been observed earlier for enzymatic degradation of DNA nanostar condensates when adding a restriction enzyme from the outside and was associated with the dynamics of the condensate and enzyme migration dynamics³⁹. Our mechanism is, however, different as the restriction enzyme is present from the start and entrapped and does not need to diffuse into the condensate. Both approaches highlight the development of RNA-mediated autonomous transient coacervate systems that function by simultaneously utilizing RNA strands and the endoribonuclease. These systems will be used below for slow activation of binary coacervate systems.

Engineering wetting between coacervates

After understanding how the combination of A_{1500} and B_x can lead to the formation of dynamic and switchable coacervates, we hypothesized that these simple-to-prepare coacervates can be used to engineer coacervate mixtures and interactions using various binders. To this end, we prepared three distinct coacervates: C_1 in magenta, C_2 in green, and C_3 in cyan, using different binders B_{8-1} , B_{8-2} , and B_{8-3} , respectively, wherein each binder is associated with a specific and selectively binding palindromic sequence (P_{8-1} , P_{8-2} , and P_{8-3} , as shown in Figs. 2b, c and 4a). After the initial formation of the individual coacervates (time = 1 h; 37 °C), we combined two of them to understand whether they remain segregated or potentially fuse despite being built by different palindromic binders.

strands into RNase H-loaded systems^{36–38}. Fig. 3g–k displays transient coacervate disassembly. Coacervates formed by A_{1500} and B_{8-1} were first generated and then combined with an excess of RNA invader (10 eq. of binder) at a low concentration of RNase H (0.1 $\text{U } \mu\text{L}^{-1}$). Before introducing the RNA invader, CLSM images show the initially formed coacervates (Fig. 3k). The subsequent simultaneous addition of RNA invader and RNase H set off an autonomous and dynamic transformation between coacervate and solution states. Within 10 min, the coacervates disassemble into a fully homogeneous solution due to rapid hybridization of B_{8-1} and RNA invader, which blocks multivalent interactions. After 0.5 h, some minor coacervates

Following an 11-day incubation period at 37 °C, a rich diversity of morphologies emerges. In general, the process follows initial contact at early times, subsequent engulfment, formation of a preferred wetting layer, and ultimately complete mixing (Fig. 4). The harmonization process occurs on different time scales for the different coacervate mixtures and is not complete for mixtures of C_1 (magenta)/ C_3 (cyan) and of C_2 (green)/ C_3 (cyan), for which distinct core-shell morphologies persist with slow homogenization even after 11 days (Fig. 4c, d). These observations are in line with the diminished dynamics of C_3 relative to C_1 and C_2 (Supplementary Fig. 2). The tendency to form the wetting layer on the surface follows $C_1 < C_2 < C_3$. It leaves us to speculate that the small differences in palindrome binder—despite being very similar in structure and thermodynamics—leads to slightly different surface tensions. It is interesting to note that the most hydrophilic dye (Atto₄₈₈) located on C_2 (green) does not form the most effective surface wetting layer (Fig. 4d). Concerning the gradual homogenization, control experiments by gel electrophoresis point to a gradual strand displacement within simplified model system of A_{37}/B_{8-1} and B_{8-2} (Supplementary Fig. 8), wherein the initially bound B_{8-1} strand is undergoing slow exchange with B_{8-2} . This process may aid in compatibilization. Note that NUPACK simulations do not indicate cross-talk/off-target binding between the different B_{8-x} binders down to a temperature of 5 °C.

To further investigate the emergence of wetting phenomena, we employed the autonomous formation of one coacervate system in the presence of an already formed different coacervate. This connects to Fig. 3c, where RNase H-mediated digestion of RNA was used to trigger coacervation. When using slow RNase H-mediated formation of C_1 in the presence of already preformed C_2 (Fig. 4e), the data shows homogeneous nucleation of distinct magenta C_1 structures in the presence of preformed C_2 . Heterogeneous nucleation is absent. Over time, these discrete coacervates form a unified coacervate. When slowly activating C_1 to preformed C_3 (Fig. 4f), again homogeneous nucleation takes place followed by the formation of core-shell structures. Hence the morphological development is independent of the nucleation pathway and the temporal orchestration. No matter whether preformed coacervates are mixed or whether one is grown slowly, similar fully mixed or core/shell structures appear. This points to the robustness of the process. Overall, this approach shows how to control diverse morphologies in the presence of two distinct coacervate systems, thereby not only achieving wetting control but also mimicking the formation processes and wetting behaviors of the biological organelles within cells^{29,40–42}.

Obviously, the wetting process between two preformed coacervates takes more than one week because of the slow mobility of the coacervates, as well as the very slow possible exchange of binder segments. To gain a better understanding of the wetting behavior and accelerate this process, we employed a so-called C_{31} system together with the C_1 coacervates (Fig. 5). The C_{31} coacervate was engineered to contain mixtures of its original B_{8-3} binder and either 25 or 50 mol% of the B_{8-1} binder (Fig. 5a). The latter serves to strengthen and accelerate interactions between the C_{31} and the C_1 .

Upon mixing C_1 and C_{31} (Fig. 5c, d), core-shell structures visually identical to the C_1/C_3 system are formed (Figs. 4c and 5b), but with different formation times, based on the ratio of B_{8-3} to B_{8-1} . C_{31} with a $B_{8-3}:B_{8-1}$ ratio of 75%:25% leads to the observation of Janus-like structures within 1 day. Following this, multicompartiment structures occur after 3 days, and the final core-shell structures emerge within 7 days (Fig. 5c). Furthermore, changing the $B_{8-3}:B_{8-1}$ ratio to 50%:50% significantly enhances the wetting behavior, resulting in the emergence of the final core-shell structures within 3 days, instead of 7 days (Fig. 5d). This phenomenon indicates that the wetting speed can be effectively modulated by tuning the multivalent interactions of the binders between two coacervates.

The wetting behavior of C_1 and C_{31} helps to understand the interaction in a mixture of pure, distinct C_1 and C_3 . In the mixture of C_1 and C_3 , as mentioned above, the unbound free A repeat units on A_{1500} within coacervates present opportunities for strand exchange between B_{8-1} in the C_1 coacervate and B_{8-3} in the C_3 coacervate (Fig. 5e; Supplementary Fig. 8). This

strand displacement process leads to an increased presence of B_{8-3} in C_1 as well as of B_{8-1} in C_3 that enables multivalent interactions between the original C_1 and C_3 via wetting and engulfment. This strand displacement behavior can occur when the coacervates come into contact. Subsequently, the strand exchange enhances the emergence of complex structures through wetting, fusion, and engulfment. The process is sketched in Fig. 5e. We hypothesize that strand exchange may also occur very slowly, even when the coacervates are at a distance from each other through complete detachment of the binders and their diffusion (equilibrium dynamics of dsDNA). It is reasonable to assume that elongation of the T_x segment in the binders would further limit the molecular exchange and thus slow down or even prevent fusion.

Conclusions

In summary, we introduced a simple and versatile platform for programmable DNA coacervates. In contrast to many other DNA coacervate systems, this model system does not require much knowledge on the design of DNA nanostars, complicated synthesis or well-designed annealing protocols, but operates on a simple mix-and-use principle. Furthermore, due to the presence of a polymeric component (polyA), a different viscoelastic regime can be generated within the coacervates as compared to nanostar-based droplets, because polymer entanglements can be present for long polyA, as well as higher multivalency effect. FRAP measurements indicate a slow and partial recovery in the coacervates, contrasting with the rapid and almost complete recovery reported in nanostar-based droplets by previous studies^{22,43–45}. Even though we synthesized the polyA building block in-house, it is commercially available, and preliminary experiments show that the commercial polyA also undergoes coacervation (Supplementary Fig. 9).

Using established strand displacement switching principles of DNA nanoscience, we demonstrated simple switching of our coacervates. The assembly/disassembly switching can also be achieved using RNA/RNase H switches that allow fine-tuning of the kinetics and the design of autonomous systems, where recruitment of the enzymes into the coacervate droplet was observed. The liquid-like properties and small differences in the palindrome binder of these coacervates paved the way for engineering wetting, clustering, engulfment, and merging of the distinct coacervate droplets. The interaction of these coacervates can be simply engineered by co-hybridization with other linkers, which should allow for sequential mixing processes in the future.

The facile tunability and the facile options for functionalization should enable fundamental studies into coacervate dynamics and structures, as well as open doors for applications in delivery, synthetic biology, and material science.

Methods

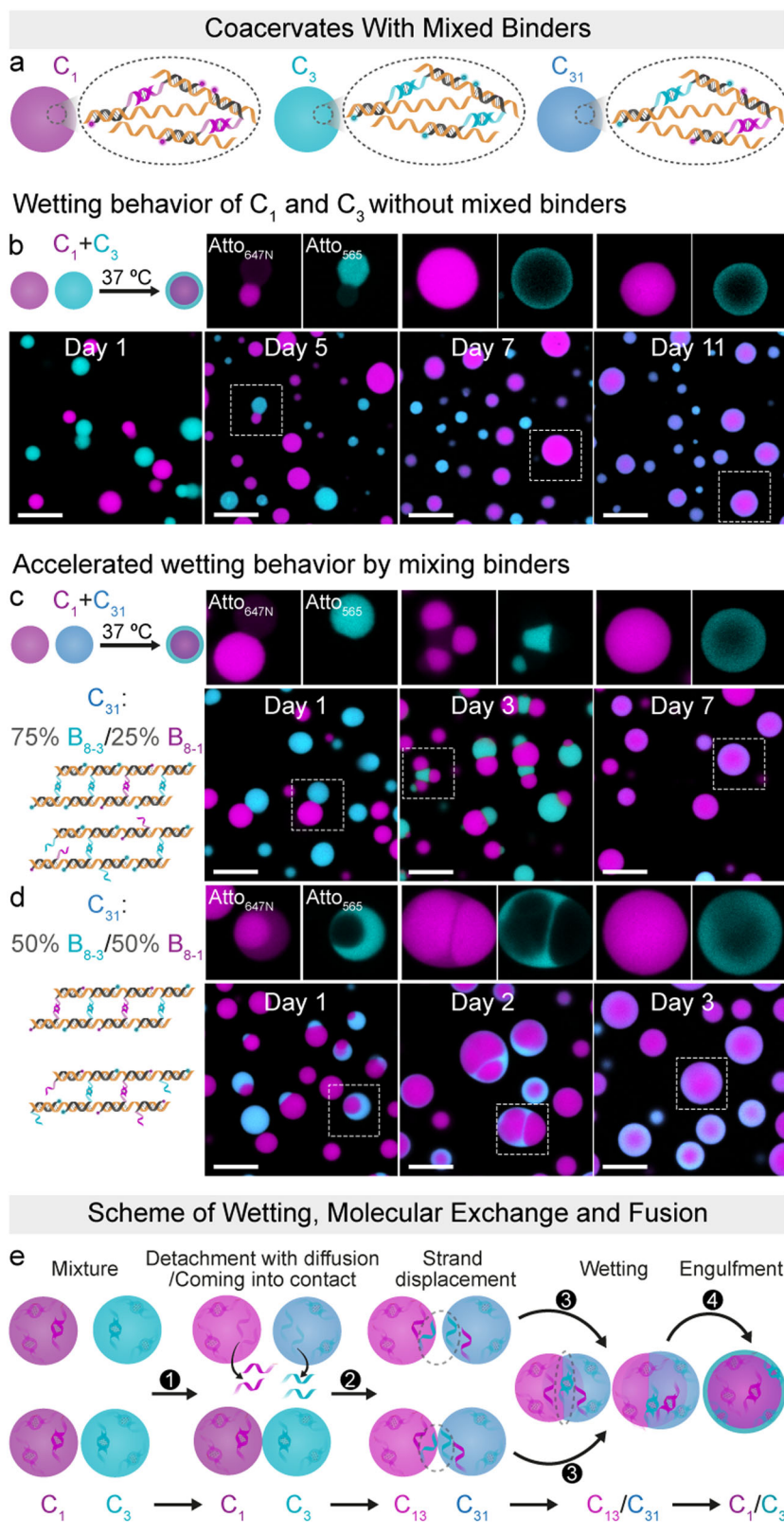
Synthesis of ssDNA polymer A_{1500} by TdT polymerization

TdT polymerization is a widely employed method for synthesizing ssDNA products through controlled nucleotide polymerization. To synthesize A_{1500} , a mixture of 0.2 μM primer, 300 μM dATP, 1x TdT buffer, and 1 U μL^{-1} TdT enzyme (Supplementary Materials) was prepared in nuclease-free water, resulting in a final volume of 150 μL . The reaction was conducted at 37 °C for 2 h and then quenched by adding 20 μL of 200 mM EDTA solution. The obtained polymer was purified using 10 kDa amicon ultra centrifugal filters and washed three times with TE buffer. The concentration of the polymer was determined using UV-Vis spectroscopy (Supplementary Characterization Methods and Instrument).

Palindromic effect on coacervate formation

To evaluate the impact of the palindromic length and GC content on the multivalency-driven coacervation, eight different binder strands with varying palindromic lengths and sequences were introduced (Supplementary Table 1). The samples were prepared by dissolving 0.03 g L^{-1} (~0.06 μM) A_{1500} and 1.5 μM binder in rCutSmart buffer containing 10 mM Mg^{2+} and 50 mM K^+ (pH = 7.9), resulting in a final volume of 20 μL . The solutions were incubated for 4 h at 37 °C with gentle rotation at 80 rpm. The

Fig. 5 | Engineering accelerated wetting between two coacervates and its mechanisms. Coacervates C_1 (or C_3) were formed using a mixture containing a final concentration of $0.06 \mu\text{M}$ of A_{1500} and $1.5 \mu\text{M}$ of either B_{8-1} or B_{8-3} . Coacervates C_{31} were generated from $0.06 \mu\text{M}$ A_{1500} and a mixture totaling $1.5 \mu\text{M}$ of B_{8-1} and B_{8-3} . **a** Illustration of three distinct coacervate structures (C_1 in magenta, C_3 in cyan, and C_{31} in dark cyan) synthesized using different binders (B_{8-1} , B_{8-3} , and a mixture of B_{8-3} and B_{8-1}). The experiments were performed at 37°C with gentle rotation at 80 rpm unless otherwise specified. **b** Wetting behavior upon the combination of C_1 and C_3 . **c** Accelerated wetting behavior upon the combination of C_1 and C_{31} by the introduction of B_{8-1} in the C_{31} system at a ratio of 75%:25% B_{8-3} : B_{8-1} ($1.125 \mu\text{M}$ of B_{8-3} and $0.375 \mu\text{M}$ of B_{8-1}). **d** Accelerated wetting behavior upon the combination of C_1 and C_{31} by introducing B_{8-1} in the C_{31} system at a ratio of 50%:50% B_{8-3} : B_{8-1} ($0.75 \mu\text{M}$ of B_{8-3} and $0.75 \mu\text{M}$ of B_{8-1}). The experiments were conducted at 37°C without rotation to minimize collisions. **e** Suggested mechanisms of coacervate fusion for C_1 and C_3 . The molecular exchange between different-type coacervates occurs through either detachment of the binders and their diffusion or strand displacement. Scale bars: $10 \mu\text{m}$.



resulting structures were visualized and recorded using CLSM. The experiments were conducted using a 384-well microtiter plate with a 0.2 mm glass bottom.

Time-dependent coacervate formation

A $20 \mu\text{L}$ solution was prepared containing $0.06 \mu\text{M}$ of A_{1500} and $1.5 \mu\text{M}$ of B_{8-1} in rCutSmart buffer. This solution was incubated for 30 h at 37°C with a

rotation of 80 rpm . The coacervate formation process was recorded using CLSM.

DNA-triggered switchable coacervate

To realize a transformation sequence from coacervate to solution and back to coacervate (coacervate-to-solution-to-coacervate), coacervates containing B_{8-1} were prepared with a final concentration of $0.06 \mu\text{M}$ A_{1500} and

1.5 μM (1.0 eq.) of B_{8-1} in rCutSmart buffer. This mixture was incubated for 12 h at 37 °C with gentle rotation at 80 rpm. Subsequently, 2.25 μM (1.5 eq.) of DNA invader was introduced and allowed to incubate for 0.5 h, resulting in the disassembly of the coacervates. Following this, 3 μM (2.0 eq.) of DNA anti-invader was added and incubated for an additional 16 h, leading to the reformation of coacervates. Images were recorded during this process using CLSM.

RNA-triggered switchable coacervate

In the switchable system between coacervate and solution states, coacervates containing B_{8-1} were prepared with a final concentration of 0.06 μM A_{1500} and 1.5 μM (1.0 eq.) of B_{8-1} in rCutSmart buffer. This mixture was incubated for 1 h at 37 °C with gentle rotation at 80 rpm. Subsequently, RNA invader (4.5 μM , 3 eq.) was introduced and allowed to incubate for 10 min until the coacervates disappeared. Following this, 0.1 $\text{U } \mu\text{L}^{-1}$ RNase H was added and incubated overnight.

For the transformation sequence of solution-to-coacervate-to-solution, a mixture containing 0.06 μM A_{1500} , 1.5 μM (1.0 eq.) B_{8-1} , and 2.25 μM (1.5 eq.) DNA invader was prepared in rCutSmart buffer (complex of A_{1500}/B_{8-1} /DNA invader). The solution was rapidly heated to 80 °C at a rate of 3 °C s^{-1} and then gradually cooled to 20 °C at a rate of 0.01 °C s^{-1} . Subsequently, RNA anti-invader (15 μM , 10.0 eq.) was added to the annealed solution and incubated for 1 h to form coacervates. Following this, 0.1 $\text{U } \mu\text{L}^{-1}$ RNase H was introduced and incubated for 2 h, resulting in the coacervates disassembling into a homogeneous solution.

RNA-regulated transient coacervate

For the RNA-regulated transient coacervate disassembly system, the coacervates were first prepared with final concentrations of 0.06 μM of A_{1500} and 1.5 μM (1.0 eq.) of B_{8-1} in rCutSmart buffer. The mixture was incubated for 2 h at 37 °C with gentle rotation at 80 rpm. Following this, varying amounts of RNA invader (15, 45, 75 μM) and 0.1 $\text{U } \mu\text{L}^{-1}$ RNase H were added to the solution. The mixture was then incubated at 37 °C with gentle rotation at 80 rpm. Images were recorded during this process using CLSM, and the tunable reassembly time was monitored. Additionally, to further explore the effect of RNase H concentration on the reassembly time, RNA invader (15 μM , 10.0 eq.) and different RNase H concentrations (0.03, 0.05, 0.1 $\text{U } \mu\text{L}^{-1}$) were introduced. The duration of reassembly is measured from the moment the preformed coacervates disassemble to the commencement of coacervate reformation.

To achieve the opposite pathway (transient coacervate assembly), RNA anti-invader and RNase H were introduced. The complex of A_{1500}/B_{8-1} /DNA invader was prepared with a final concentration of 0.06 μM A_{1500} , 1.5 μM (1.0 eq.) B_{8-1} , and 2.25 μM (1.5 eq.) DNA invader in rCutSmart buffer. The solution was rapidly heated to 80 °C at a rate of 3 °C s^{-1} and then gradually cooled to 20 °C at a rate of 0.01 °C s^{-1} . Then different concentrations of RNA anti-invader (15, 45 μM) and RNase H (0.1 $\text{U } \mu\text{L}^{-1}$) were added to the solution. The mixture was incubated at 37 °C with gentle rotation at 80 rpm, and images were recorded during this process using CLSM.

Engineering wetting between coacervates

Three distinct coacervate structures, denoted as C_1 , C_2 , and C_3 , were prepared using different binders (B_{8-1} , B_{8-2} , and B_{8-3}). A mixture with a final concentration of 0.06 μM A_{1500} and 1.5 μM of the respective B_x was dissolved in rCutSmart buffer and incubated for 1 h at 37 °C with gentle rotation at 80 rpm. Subsequently, two of these resulting coacervates were mixed and incubated for 11 days at 37 °C without shaking (shaking was avoided in this case to limit collisions). The morphological changes during this period were captured and recorded using CLSM.

Engineering wetting under nucleation process by activating C_1 to preformed C_2 (or C_3)

To investigate the structures that can emerge through the wetting behavior during the nucleation process, we introduced a system where B_{8-1} is blocked by an RNA invader. Coacervates of C_2 and C_3 were

prepared as described previously. A mixture consisting of A_{1500} (0.06 μM), B_{8-1} (1.5 μM , 1.0 eq.), and RNA invader (2.25 μM , 1.5 eq.) was prepared in rCutSmart buffer, forming the complex of $A_{1500}/B_{8-1}/\text{RNA}$ invader. The solution was rapidly heated to 80 °C at a rate of 3 °C s^{-1} and then gradually cooled to 20 °C at a rate of 0.01 °C s^{-1} . Subsequently, 0.1 $\text{U } \mu\text{L}^{-1}$ RNase H and preformed C_2 (or C_3) were introduced into the solution and incubated for 72 h at 37 °C with gentle rotation at 80 rpm. The morphological changes occurring during this period were monitored and recorded using CLSM.

Accelerated wetting between two coacervates

To facilitate the wetting process, coacervate C_{31} , incorporating different ratios of B_{8-1} and B_{8-3} ($B_{8-3}:B_{8-1} = 75\%:25\%$, 50%:50%), was employed. In the system with 75%:25% $B_{8-3}:B_{8-1}$, a mixture comprising 1.125 μM of B_{8-3} and 0.375 μM of B_{8-1} was combined with 0.06 μM A_{1500} in rCutSmart buffer. This solution was then incubated for 1 h at 37 °C with gentle rotation at 80 rpm to form C_{31} . C_1 was prepared as described previously. Subsequently, C_{31} solution was mixed with the C_1 solution and incubated for 7 days at 37 °C without shaking. Morphological changes during this period were observed and recorded using CLSM.

Strand exchange reaction between A_{37}/B_{8-1} and B_{8-2}

A mixture was prepared by mixing 2 μM A_{37} and 10 μM B_{8-1} in rCutSmart buffer, resulting in a final volume of 20 μL . This solution was rapidly heated to 80 °C at a rate of 3 °C s^{-1} and then slowly cooled to 20 °C at a rate of 0.01 °C s^{-1} . Then 10 μM B_{8-2} was added to the solution, and the mixture was incubated for 24 h at 37 °C. The samples were analyzed through agarose gel electrophoresis using a 4 wt% agarose gel.

Coacervate formation using commercial polyA

A 20 μL solution containing 0.06 μM of polyA and 2.5 μM of B_{8-1} in rCutSmart buffer was prepared. This solution was incubated at 37 °C with a rotation of 80 rpm, and images were recorded during this process using CLSM.

Reporting summary

Further information on research design is available in the Nature Portfolio Reporting Summary linked to this article.

Data availability

The authors declare that all relevant data supporting the findings of this study are available within the paper and its Supplementary Information file. The source data for Figs. 2c and 3h-j are included in Supplementary Data 1. Additional data related to this study are available from the corresponding author upon reasonable request.

Received: 2 November 2023; Accepted: 19 April 2024;

Published online: 01 May 2024

References

- Banani, S. F., Lee, H. O., Hyman, A. A. & Rosen, M. K. Biomolecular condensates: organizers of cellular biochemistry. *Nat. Rev. Mol. Cell Biol.* **18**, 285–298 (2017).
- Garabedian, M. V. et al. Designer membraneless organelles sequester native factors for control of cell behavior. *Nat. Chem. Biol.* **17**, 998–1007 (2021).
- Gomes, E. & Shorter, J. The molecular language of membraneless organelles. *J. Biol. Chem.* **294**, 7115–7127 (2019).
- Hernandez-Verdun, D. Assembly and disassembly of the nucleolus during the cell cycle. *Nucleus* **2**, 189–194 (2011).
- Mao, Y. S., Zhang, B. & Spector, D. L. Biogenesis and function of nuclear bodies. *Trends Genet.* **27**, 295–306 (2011).
- Decker, C. J. & Parker, R. P-Bodies and stress granules: possible roles in the control of translation and mRNA degradation. *Cold Spring Harb. Perspect. Biol.* **4**, a012286 (2012).

7. Kaur, T. et al. Sequence-encoded and composition-dependent protein-RNA interactions control multiphasic condensate morphologies. *Nat. Commun.* **12**, 872 (2021).
8. Liu, W., Samanta, A., Deng, J., Akintayo, C. O. & Walther, A. Mechanistic insights into the phase separation behavior and pathway-directed information exchange in all-DNA droplets. *Angew. Chem. Int. Ed.* **61**, e202208951 (2022).
9. Milovanovic, D., Wu, Y., Bian, X. & Camilli, P. D. A liquid phase of synapsin and lipid vesicles. *Science* **361**, 604–607 (2018).
10. Hirose, T., Ninomiya, K., Nakagawa, S. & Yamazaki, T. A guide to membraneless organelles and their various roles in gene regulation. *Nat. Rev. Mol. Cell Biol.* **24**, 288–304 (2023).
11. Beutel, O., Maraschini, R., Pombo-García, K., Martin-Lemaitre, C. & Honigsmann, A. Phase separation of zonula occludens proteins drives formation of tight junctions. *Cell* **179**, 923–936 (2019).
12. Schuster, B. S. et al. Controllable protein phase separation and modular recruitment to form responsive membraneless organelles. *Nat. Commun.* **9**, 2985 (2018).
13. Yewdall, N. A., André, A. A. M., Lu, T. & Spruijt, E. Coacervates as models of membraneless organelles. *Curr. Opin. Colloid Interface Sci.* **52**, 101416 (2021).
14. Hyman, A. A., Weber, C. A. & Jülicher, F. Liquid–liquid phase separation in biology. *Annu. Rev. Cell Dev. Biol.* **30**, 39–58 (2014).
15. Liu, W., Lupfer, C., Samanta, A., Sarkar, A. & Walther, A. Switchable hydrophobic pockets in DNA protocells enhance chemical conversion. *J. Am. Chem. Soc.* **145**, 7090–7094 (2023).
16. Leathers, A. et al. Reaction-diffusion patterning of DNA-based artificial cells. *J. Am. Chem. Soc.* **144**, 17468–17476 (2022).
17. Cook, A. B., Novosedlik, S. & van Hest, J. C. M. Complex coacervate materials as artificial cells. *Acc. Mater. Res.* **4**, 287–298 (2023).
18. Lu, T. et al. Endocytosis of coacervates into liposomes. *J. Am. Chem. Soc.* **144**, 13451–13455 (2022).
19. te Brinke, E. et al. Dissipative adaptation in driven self-assembly leading to self-dividing fibrils. *Nat. Nanotechnol.* **13**, 849–855 (2018).
20. Spruijt, E. Open questions on liquid–liquid phase separation. *Commun. Chem.* **6**, 23 (2023).
21. Wang, J., Li, Z. & Willner, I. Dynamic reconfigurable DNA nanostructures, networks and materials. *Angew. Chem. Int. Ed.* **62**, e202215332 (2023).
22. Sato, Y., Sakamoto, T. & Takinoue, M. Sequence-based engineering of dynamic functions of micrometer-sized DNA droplets. *Sci. Adv.* **6**, eaba3471 (2020).
23. Merindol, R., Loescher, S., Samanta, A. & Walther, A. Pathway-controlled formation of mesostructured all-DNA colloids and superstructures. *Nat. Nanotechnol.* **13**, 730–738 (2018).
24. Samanta, A., Hömer, M., Liu, W., Weber, W. & Walther, A. Signal-processing and adaptive prototissue formation in metabolic DNA protocells. *Nat. Commun.* **13**, 3968 (2022).
25. Samanta, A., Sabatino, V., Ward, T. R. & Walther, A. Functional and morphological adaptation in DNA protocells via signal processing prompted by artificial metalloenzymes. *Nat. Nanotechnol.* **15**, 914–921 (2020).
26. Jeon, B.-j., Nguyen, D. T. & Saleh, O. A. Sequence-controlled adhesion and microemulsification in a two-phase system of DNA liquid droplets. *J. Phys. Chem. B* **124**, 8888–8895 (2020).
27. Deng, J. & Walther, A. Programmable and chemically fueled DNA coacervates by transient liquid–liquid phase separation. *Chem* **6**, 3329–3343 (2020).
28. Sato, Y. & Takinoue, M. Sequence-dependent fusion dynamics and physical properties of DNA droplets. *Nanoscale Adv.* **5**, 1919–1925 (2023).
29. Mangiarotti, A., Chen, N., Zhao, Z., Lipowsky, R. & Dimova, R. Wetting and complex remodeling of membranes by biomolecular condensates. *Nat. Commun.* **14**, 2809 (2023).
30. Deng, J. & Walther, A. ATP-powered molecular recognition to engineer transient multivalency and self-sorting 4D hierarchical systems. *Nat. Commun.* **11**, 3658 (2020).
31. Rubio-Sánchez, R., Mognetti, B. M., Cicuta, P. & Di Michele, L. DNA-origami line-actants control domain organization and fission in synthetic membranes. *J. Am. Chem. Soc.* **145**, 11265–11275 (2023).
32. Li, Z. et al. Dynamic fusion of nucleic acid functionalized nano-/micro-cell-like containments: from basic concepts to applications. *ACS Nano* **17**, 15308–15327 (2023).
33. Heinen, L. & Walther, A. Celebrating soft matter’s 10th anniversary: approaches to program the time domain of self-assemblies. *Soft Matter* **11**, 7857–7866 (2015).
34. Tang, L., Navarro, L. A. Jr, Chilkoti, A. & Zauscher, S. High-molecular-weight polynucleotides by transferase-catalyzed living chain-growth polycondensation. *Angew. Chem. Int. Ed.* **56**, 6778–6782 (2017).
35. Fowler, J. D. & Suo, Z. Biochemical, structural, and physiological characterization of terminal deoxynucleotidyl transferase. *Chem. Rev.* **106**, 2092–2110 (2006).
36. Green, L. N. et al. Autonomous dynamic control of DNA nanostructure self-assembly. *Nat. Chem.* **11**, 510–520 (2019).
37. Sun, M., Deng, J. & Walther, A. Communication and cross-regulation between chemically fueled sender and receiver reaction networks. *Angew. Chem. Int. Ed.* **62**, e202214499 (2023).
38. Farag, N., Dordevic, M., Del Grosso, E. & Ricci, F. Dynamic and reversible decoration of DNA-based scaffolds. *Adv. Mater.* **35**, 2211274 (2023).
39. Saleh, O. A., Jeon, B. J. & Liedl, T. Enzymatic degradation of liquid droplets of DNA is modulated near the phase boundary. *PNAS* **117**, 16160–16166 (2020).
40. Yoo, B. Y. & Chrispeels, M. J. The origin of protein bodies in developing soybean cotyledons: a proposal. *Protoplasma* **103**, 201–204 (1980).
41. Ambroggio, E. E., Costa Navarro, G. S., Pérez Socas, L. B., Bagatolli, L. A. & Gamarnik, A. V. Dengue and Zika virus capsid proteins bind to membranes and self-assemble into liquid droplets with nucleic acids. *J. Biol. Chem.* **297**, 101059 (2021).
42. Snead, W. T. et al. Membrane surfaces regulate assembly of ribonucleoprotein condensates. *Nat. Cell Biol.* **24**, 461–470 (2022).
43. Agarwal, S., Osmanovic, D., Dizani, M., Klocke, M. A. & Franco, E. Dynamic control of DNA condensation. *Nat. Commun.* **15**, 1915 (2024).
44. Maruyama, T., Gong, J. & Takinoue, M. Temporally controlled multistep division of DNA droplets for dynamic artificial cells. Preprint at *ChemRxiv* <https://doi.org/10.26434/chemrxiv-2024-z67br> (2024).
45. Skipper, K. & Wickham, S. Core–shell coacervates formed from DNA nanostars. Preprint at *ChemRxiv* <https://doi.org/10.26434/chemrxiv-2024-07pvd> (2024).

Acknowledgements

This work was supported by the DFG in WA 3084/19-1. W. L. acknowledges the support by the Chinese Scholarship Council (CSC).

Author contributions

W.L. and A.W. conceived the project, designed the experiments, analyzed the data, and wrote the manuscript. W.L. performed the experiments and collected the data. J.D. contributed to the project design and data analysis. S. Song conducted experiments for synthesizing commercial polyA-based coacervates and supported the interpretation of the results. S. Sethi assisted with the discussions of the results. A.W. supervised the work.

Funding

Open Access funding enabled and organized by Projekt DEAL.

Competing interests

The authors declare no competing interests.

Additional information

Supplementary information The online version contains supplementary material available at

<https://doi.org/10.1038/s42004-024-01185-4>.

Correspondence and requests for materials should be addressed to Andreas Walther.

Peer review information *Communications Chemistry* thanks the anonymous reviewers for their contribution to the peer review of this work. A peer review file is available.

Reprints and permissions information is available at <http://www.nature.com/reprints>

Publisher's note Springer Nature remains neutral with regard to jurisdictional claims in published maps and institutional affiliations.

Open Access This article is licensed under a Creative Commons Attribution 4.0 International License, which permits use, sharing, adaptation, distribution and reproduction in any medium or format, as long as you give appropriate credit to the original author(s) and the source, provide a link to the Creative Commons licence, and indicate if changes were made. The images or other third party material in this article are included in the article's Creative Commons licence, unless indicated otherwise in a credit line to the material. If material is not included in the article's Creative Commons licence and your intended use is not permitted by statutory regulation or exceeds the permitted use, you will need to obtain permission directly from the copyright holder. To view a copy of this licence, visit <http://creativecommons.org/licenses/by/4.0/>.

© The Author(s) 2024